Sustainable Cities and Society 107 (2024) 105446

Contents lists available at ScienceDirect

Sustainable Cities and Society

journal homepage: www.elsevier.com/locate/scs

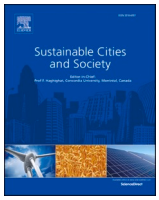

Enhancing smart city operation management: Integrating energy systems with a subway synergism hub

Mahmoud Roustaei [a,b], Taher Niknam [a], Jamshid Aghaei [c,*], Morteza Sheikh [a], Hossein Chabok [a], Abdollah Kavousi-Fard [a], Vahid Vahidinasab [d], Josep M. Guerrero [e]

[a] Department of Electrical and Electronics Engineering, Shiraz University of Technology, Shiraz, Iran
[b] Fars Province Electrical Distribution Company, Shiraz, Iran
[c] School of Engineering and Technology, Central Queensland University, Rockhampton, Australia
[d] Department of Engineering at Nottingham Trent University (NTU), UK
[e] Faculty of Engineering and Science and at the Department of Energy Technology, Aalborg University, Denmark

ARTICLE INFO

Keywords:
Subway synergism hub
Smart city
Microgrid
Directed acyclic graph
IPS algorithm

ABSTRACT

This paper is centered on establishing a secure framework for the optimal concurrent operation of a smart city, encompassing transportation, water, heat, electrical, and cooling energy systems. The studied smart city includes the microgrid, smart transportation system (STS), energy hub (EH) and smart grid. In this regard, a subway synergism hub (SSH) as a new non-energy system is added to the smart city with the aim of serving the subway's water, heat, electrical and cooling demands as well as diminishing the operation cost of the smart city. The EH within the SSH cooperated with a desalination unit is considered to supply the subway's stations water demand by using the sea water. The investigation of the optimal allocation of the SSH unit for reducing the cost of smart city operation is also conducted by introducing a novel intelligent priority selection (IPS) analytical algorithm. In comparison to common meta-heuristic algorithms for allocation problems, the accurate optimal solution can be found in low runtime by the IPS algorithm. To achieve an accurate model of the smart city, directed acyclic graph (DAG) based blockchain approach is provided which can enhance the data and energy exchanges security within the smart city. This research paper introduces a security framework deployed in a smart city setting to establish a secure platform for energy transactions. The findings validate the effectiveness of this model and highlight the value of the IPS method. The effectiveness of the suggested approach has been assessed using the smart city system is comprised of various sections, including EVs, smart grid, microgrid, and SSH, demonstrating the credibility and accuracy of this study.

1. Introduction

1.1. Motivation and aims

Cities now play a crucial role in addressing significant societal and economic challenges, such as promoting the adoption of environmentally friendly practices, reducing harmful emissions, improving energy conservation, and implementing distributed energy resources (DER), all while fostering economic growth (Liang et al., 2024). The concept of the smart city aims to enhance the performance and efficiency of urban amenities, including utilities and transportation by implementing communication infrastructure and smart devices to reduce resource consumption, waste, and overall costs (Bridge et al., 2013). Smart cities emphasize the interconnectedness of systems, with a particular focus on communication and technology (Hui et al., 2023). Previous studies (Mwasilu et al., 2014; Calvillo et al., 2016) have classified various types of intervention zones within smart cities. The aim of the paper is to propose a secure and robust synergy mechanism that ensures the efficient functioning of the transportation system while maintaining data privacy and protection against cyber threats to enable seamless connectivity, real-time data exchange, and intelligent decision-making.

1.2. Literature review and research gaps

The current works in the literature can be classified into several categories, highlighting the research gaps in each area:

Synergies for addressing energy demand in urban areas: The concept of

* Corresponding author.
E-mail address: j.aghaei@cqu.edu.au (J. Aghaei).

https://doi.org/10.1016/j.scs.2024.105446
Received 28 December 2023; Received in revised form 14 March 2024; Accepted 15 April 2024
Available online 25 April 2024

Nomenclature

Sets/Indices

ϑ^s/s Set and index of metro's stations, ϑ^s ={1, …,6}.
ϑ^{fl}/f Set and index of EV parking fleets, ϑ^{fl}= {1,…,6}.
ϑ^i/i Set and index of H_{w_i}, ϑ^i= {1,..,m}.
ϑ^j/j Set and index of the iteration number.
ϑ^m/m Set and index of matrix W components.
ϑ^M/M Set and index related to the matrix $K^{''}$, ϑ^M= {1,..,n}.
ϑ^N/N Set and index of subway's stations candidates.
ϑ^n/n Set and index of control variable for the optimization allocation algorithm.
ϑ^κ/κ Set and index of uncertainty sources.
ϑ^u/u Set and index of urban transportation paths, ϑ^u = {1,…, 12}.
ϑ^t/t Set and index of time intervals.

Constants

$Bp1^s_v$,$Bp2^s_v$, $Bp2^s_i$ Bidding prices of E2G, E2SSH, SSH2E (SSH2G) energy exchanges.
B^v_{deg} The degradation cost of EVs battery.
$C^{Boi}_s/C^T_s/C^{CHP}_s/C^{Ch}_s$ Rated capacity of the boiler/transformer/ CHP, Boiler and absorption chiller.
$\underline{E}^v, \overline{E}^v$ Battery capacity range of EVs: min and max.
$Ec^{s,u}$ EV's energy consumption to travel across the k^{th} path to the s^{th} station.
$\underline{P}^f_{Ec}$,$\overline{P}^f_{Ec}$ Range of EVs' battery charging rate: min and max.
$\underline{P}^f_{Ed}$,$\overline{P}^f_{Ed}$ Range of EVs' battery discharging rate: min and max..
$P^{E_{eh}}_{s,t}$,$P^{H_{eh}}_{s,t}$,$P^{C_{eh}}_{s,t}$ Electrical, thermal and cooling demands of Subway at the time t, respectively.
$\underline{P}^{ES}_s$, $\overline{P}^{ES}_s$ Range of battery charging rates: min and max.
P Matrix of potential metro station locations.
$\underline{P}^{EH}$, $\overline{P}^{EH}$,$\underline{S}^{ES}$, $\overline{S}^{ES}$ Min and max of EH's power exchange and battery charger level, respectively.
$\underline{Vol}^{ST}_s$,$\overline{Vol}^{ST}_s$ Min/max volume of secondary tank.
$\overline{Vol}^{DT}_s$ Max volume of desalination tank.
$\underline{W}^{ID}_s$, $\overline{W}^{ID}_s$ Min/max input water of desalination tank.
$\overline{W}^{OD}_s$ Max output water of desalination unit.
η^T_e,η^{GtoH}_{boi},η^{GtoH}_{chp},η^{GtoE}_{chp},η^C,η^{ch}_e,η^{dch}_e Efficiency of electric transformer, boiler's gas-to-heat conversion, CHP's gas-to-heat conversion and gas-to-electricity conversion, absorption chiller, charging and discharging of battery, respectively.

Variables

$cost^f_{\text{deg}}$,$cost_{Grid}$, $cost_{SUB}$, $cost_{water}$, $cost_{Gas}$ EVs degradation, Grid, subway, water and Gas demand supply costs, repectively.
$cost_{Inv}$ Investment cost of SSH elements.
CF^{Des} The consumed energy factor of desalination unit.
$Ev^{f,t}_1$,$Ev^{f,t}_2$,$Ev^{f,t}$ EV's battery capacity for E2G, E2SSH modes and total exchanging energy, respectively.
F Matrix of objective functions
F^{best_sort} Sorted best values of the objective function matrix.
$F1_r$ Objective function associated with each element in a matrix ψ_r
$F1_{Best}$ Optimal matrix solution of Fl_r
H_{w_i} Matrix of $k^{'}_n$
K Matrix of control variables.
KT Matrix of replaced elements in the optimization algorithm.
$k^{'}, k^{''}$ Auxiliary variables of the optimization algorithm.
$I^{ch}_{s,t}$,$I^{dch}_{s,t}$ Binary variables of (dis) charging modes of storages in EH.
$Prof_E$, $Prof_{E2G}$,$Prof_{SSH2E}$ EVs, E2G and SSH2E energy exchanges profits.
$P^{f,t}_{E2G}$,$P^{f,t}_{E2SSH}$ E2G and E2SSH energy exchanges, respectively.
$P^{s,u,f,t}_{E2SSH\_c}$,$P^{s,u,f,t}_{E2SSH\_d}$ (Dis)charging power during E2SSH mode, respectively.
$P^{u,f,t}_{E2G\_c}$, $P^{u,f,t}_{E2G\_d}$ (Dis)charging power during E2G mode, respectively.
$P^{s,u,f,t}_{Ec}$,$P^{s,u,f,t}_{Ed}$ Rated (dis)charging power of vehicle v, respectively.
$P^{s,t}_{SSH2G}$,$P^{s,t}_{G2SSH}$ SSH2G and G2SSH energy exchanges, respectively.
$P^{s,t}_{rg}$ Max braking energy of metro.
$P^{EH}_{s,t}$ SSH transacted power with grid at the time t.
$P^{GasIN}_{s,t}$ SSH gas input power at the time t.
$P^{Gas_{chp}}_{s,t}$,$P^{Gas_{boi}}_{s,t}$ Input gas power of CHP and boiler at the time t, respectively.
$P^{H_{Total}}_{s,t}$ Generated heat power of CHP and Boiler at the time t, respectively.
$P^{ch}_{s,t}/P^{dch}_{s,t}$ (Dis)charging power of the battery at the time t.
$P^{Des}_{s,t}$ Power Consumption of desalination unit at the time t.
$S^{ES}_{s,t}$ Remained energy of SSH battery at the time t.
Q_λ,Q_ζ Input and output covariance matrix, respectively.
$u^{s,u,f,t}_{Ec}$, $u^{s,u,f,t}_{Ed}$, $um^{j,u,f,t}$ Binary variables of (dis)charging modes of EVs.
$Vol^{ST}_{s,t}$ Water volume of secondary tank at the time t.
$Vol^{DT}_{s,t}$ Water volume of desalination unit tank at the time t.
$W^{OD}_{s,t}$ Output water of desalination unit at the time t.
$W^{Out}_{s,t}$ Output water of secondary tank at the time t.
$W^{ID}_{s,t}$ Input water of desalination unit at the time t.
$w^{'}_j$ Sorted matrix of W composed by the best values of objective function.
$z^{s,u,f,t}$ Binary variable pertaining to the urban paths.
p Number of uncertain variables in stochastic modeling.
ψ_r Auxiliary matrix in optimization algorithm.
ψ^{Best} Best member of matrix ψ_r based on best values of the objective function.
ζ, λ Stochastic output and input vectors, respectively.
$\overline{\zeta}$ Average value of uncertain parameters.
α^{loss}_e Loss efficiency of EH storage.
η_c, η_d (Dis)charging efficiencies, respectively.
ω Weighing factor in the stochastic modeling.

Abbreviations

DER distributed energy resources
EVs electric vehicles
DAG Directed Acyclic Graph
EHs energy hubs
SSH subway synergism hub
STSs smart transportation systems
CHP combined heat and power
BE breaking energy
HA hash address
DAEMC Data and Energy Management Center

synergies is identified as a promising approach to tackle the challenges of energy demand in cities (Morvaj et al., 2011). However, there is a need for further research to explore and develop effective strategies for implementing synergistic solutions.

Integration of electric vehicles (EVs) and renewable energy sources: The integration of EVs and DERs such as wind turbines (WTs) and photovoltaic (PV) systems introduces complexities and uncertainties (Khosrojerdi et al., 2016; Pournazarian et al., 2019). The Vehicle-to-Grid (V2G) technology shows promise in injecting surplus energy from EVs into the grid (Khosrojerdi et al., 2016; Pournazarian et al., 2019), but more research is needed to address technical challenges and constraints associated with V2G implementation (Xu et al., 2022). Moreover, the implications of EVs as controllable units regulated by aggregators need to be further investigated, including their role in power system operation and the potential for serving as energy consumers and portable storage sources (Khodayar et al., 2012).

Energy optimization in urban rail systems: Regenerative braking systems in urban metro systems offer opportunities for energy storage (Khayyam et al., 2015). Techniques such as regenerative braking, scheduling optimization, energy storage, and reversible stations have been proposed to improve the efficiency of utilizing train energy (González-Gil et al., 2014; Khayyam et al., 2015; Adinolfi et al., 1998; Yang et al., 2014). However, the cost of energy storage devices and the synchronization of railways remain challenges (Aguado et al., 2016; Calvillo et al., 2017).

Multi-carrier power systems and energy hubs: The development of energy hubs (EHs) in smart cities, integrating thermal, electrical, and gas infrastructures, presents opportunities for meeting diverse energy demands (Geidl et al., 2007). These EH systems have the potential to enhance electricity usage and reduce environmental impact (Xiaping et al., 2015). However, it is needed to explore interoperabilities and address the various challenges associated with multi-carrier power schemes.

Communication systems and information security in smart cities: Significant progress has been achieved in smart cities to address their communication systems and electrical, thermal, gas, and water demands (Guo et al., 2021). For instance, the operation of a smart energy hub (EH) has been examined within a smart grid model aimed at minimizing operational costs (Roustai et al., 2018). However, ensuring the security of communication systems and information exchange is crucial in smart cities (Mehdizadeh & Taghizadegan, 2017). Blockchain technology has been identified as a potential solution for enhancing information security and trustworthiness (Ashley & Johnson, 2018). Its application in microgrids has shown promise in preventing fraud and reducing operational costs (Sarda et al., 2018). A Directed Acyclic Graph (DAG) based approach has been proposed to ensure the cyber safety of energy trading in microgrids (Wang et al., 2019). However, further research is needed to explore the full potential and address the specific requirements of blockchain-based solutions in smart city contexts.

1.3. Features and capabilities

According to the above survey, while existing literature has provided valuable insights and proposed various solutions, there are several research gaps that need to be addressed. The smart cities face two significant challenges in managing energy within the transportation system, namely: 1) the increased load demands of EVs during peak traffic times, and 2) meeting the water, heating, electrical, and cooling demands of subway stations. Conversely, energy hub systems have the capability to address these energy gaps within the transportation system, thanks to their two key properties: 1) providing the necessary electrical, thermal, and water supply, and 2) offering flexibility in terms of location. These include developing effective strategies for implementing synergistic approaches, addressing technical challenges and constraints in integrating EVs and renewable energy sources, optimizing energy utilization in urban rail systems, exploring efficient transformation systems for multi-carrier power schemes, and ensuring secure communication and information exchange in smart cities using technologies such as blockchain. Accordingly, this paper aims to present a comprehensive management framework for water, heat, and cooling energy within the scope of smart city initiatives. To achieve this, a new unit called *subway synergism hub* (SSH) is introduced, which enables coordinated operations between the EH, smart transportation systems (STSs), EVs, microgrid, and smart grid. In summary, the main contributions of this paper are as follows: (i) proposing a comprehensive management framework aimed at optimizing the operational efficiency of smart cities. This framework introduces a novel unit of SSH within the existing infrastructure, with the goal of integrating sustainable practices and advanced technologies to enhance the overall functionality and sustainability of the urban environment, (ii) Enabling simultaneous operation and optimization of water, heat, cooling, and electrical energy systems in the smart city, (iii) Proposing an innovative mathematical optimization algorithm to effectively tackle the allocation challenges encountered by the SSH in the smart cities, (iv) Developing an integrated model of the smart city that consider traffic congestion and recharging infrastructure along various paths of the STSs, and (v) Developing a secure framework for energy and data transactions among different sections of the smart city.

The rest of the paper is as follows: The mathematical formulations of the city are referred to in Section II. The security framework is described in Section III. Section IV shows the intelligent priority selection algorithm and result is provided in section V.

2. Mathematical formulation of smart city

The smart city ecosystem depicted in Fig. 1 is explained here. Mathematical formulations of energy exchanges (E2G, E2S and SSH2G) and smart city EH operations are defined as follows:

2.1. E2G & E2SSH definition

EVs can exchange energy with the grid to maximize their advantages. The main benefit of EVs, as explained, can be divided into three parts. The first part, denoted as E2G, is described in (1). The second part, called E2SSH, is discussed in (3). The proposed model represents the benefit as a negative value or indicates the operating cost if it's positive. The third component of the model represents the expenses related to the EV's battery, as mentioned in (4). In (5) and (6), the energy capacity of the batteries is separately presented for grid-connected and subway-connected systems.

Traffic jams are caused by the specific interaction among drivers and vehicles, as well as the physical elements of roads and public environments. This is due to the variations in both drivers' behavior and vehicle specifications. As a result, vehicles do not exhibit uniform behavior in traffic jams, and two traffic jams may behave differently even in identical situations. The congestion of traffic flow increases travel time and reduces driving efficiency, particularly for electric vehicles (EVs), which operate at non-economical speeds, leading to significant power consumption and charging demands. However, implementing recharge lines on roads can effectively offset the power consumed by traffic jams. Therefore, recharge line technology has the potential to enhance EV consumption, resulting in more efficient energy management within smart city transportation systems. $Ec_{s,u}$is the energy used by EVs because of the traffic in urban regions and $Et_{s,u}$ is the power produced by recharging lines (6). The limitations regarding the load and unload of EVs are (7)-(16) (Kavousi-Fard et al., 2015).

– *Objective functions*

$$Prof_E = Prof_{E2G} + Prof_{E2SSH} - \sum_{f\in\theta^{fl}} Cost_f^{deg} \quad (1)$$

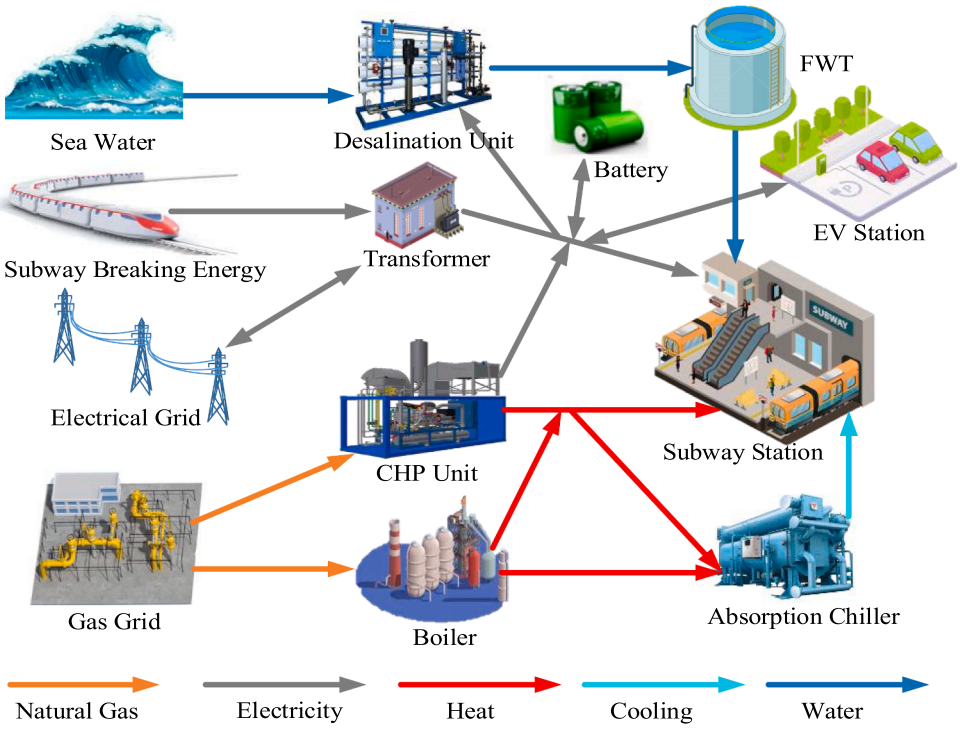

Fig. 1. Illustrative representation of the smart city.

$$Prof_{E2G} = \sum_{t\in\vartheta^t, f\in\vartheta^{fl}} \left(Bp1_{f,t} \times P^{E2G}_{f,t}\right) \tag{2}$$

$$Prof_{E2SSH} = \sum_{t\in\vartheta^t, f\in\vartheta^{fl}} \left(Bp2_{f,t} \times P^{\mathrm{E2SSH}}_{f,t}\right) \tag{3}$$

$$Cost^{deg}_f = B^{deg}_f \times \sum_{s\in\vartheta^s, u\in\vartheta^u, t\in\vartheta^t} h\left(P^{u,f,t}_{E2G\_d} + P^{s,u,f,t}_{E2SSH\_d}\right), \quad \forall f \in \vartheta^{fl} \tag{4}$$

– *Constraints*

$$Ev^1_{f,t} = Ev^1_{f,t-1} + P^{E2G\_c}_{u,f,t} \times \eta_c - P^{E2G\_d}_{u,f,t} \times \eta_d \quad \forall u \in \vartheta^u, \forall f \in \vartheta^{fl}, \forall t \in \vartheta^t \tag{5}$$

$$Ev^2_{f,t} = Ev^2_{f,t-1} + \sum_{s\in\vartheta^s, u\in\vartheta^u} \left(P^{s,u,f,t}_{E2SSH\_c} \times \eta_c - P^{s,u,f,t}_{E2SSH\_d} \times \eta_d\right) - \sum_{s\in\vartheta^s, u\in\vartheta^u} z_{s,u,f,t} \times \left(Ec_{s,u} - Et_{s,u}\right), \forall f \in \vartheta^{fl}, \forall t \in \vartheta^t \tag{6}$$

$$Ev_{f,t} = Ev^1_{f,t} + Ev^2_{f,t} \qquad \forall f \in \vartheta^{fl}, t \in \vartheta^t \tag{7}$$

$$P^{E2G}_{f,t} = Ev^1_{f,t} - Ev^1_{f,t-1} \qquad \forall f \in \vartheta^{fl}, t \in \vartheta^t \tag{8}$$

$$P^{E2SSH}_{f,t} = Ev^2_{f,t} - Ev^2_{f,t-1} \qquad \forall f \in \vartheta^{fl}, t \in \vartheta^t \tag{9}$$

$$u^{Ec}_{s,u,f,t} + u^{Ed}_{s,u,f,t} = um_{s,u,f,t} \qquad \forall s \in \vartheta^s, \forall t \in \vartheta^t, \forall f \in \vartheta^{fl}, t \in \vartheta^t \tag{10}$$

$$u^{Ec}_{s,u,f,t}\underline{P}^{Ec}_f \le P^{Ec}_{s,u,f,t} \le u^{Ec}_{s,u,f,t}\overline{P}^{Ec}_f \quad \forall s \in \vartheta^s, u \in \vartheta^u, \forall f \in \vartheta^{fl}, \forall t \in \vartheta^t \tag{11}$$

$$u^{Ed}_{s,u,f,t}\underline{P}^{Ed}_f \le P^{Ed}_{s,u,f,t} \le u^{Ed}_{s,u,f,t}\overline{P}^{Ed}_f \quad \forall s \in \vartheta^s, u \in \vartheta^u, \forall f \in \vartheta^{fl}, \forall t \in \vartheta^t \tag{12}$$

$$\underline{E}_f \le Ev_{f,t} \le \overline{E}_f \qquad \forall f \in \vartheta^{fl}, t \in \vartheta^t \tag{13}$$

2.2. Subway synergism hub definition

In the smart city context, efforts have been made to establish a synergy mechanism for supplying water, heat, cooling, and electricity. A crucial aspect to consider is the energy balancing of the SSH unit. This balancing involves various sources such as breaking energy (BE), combined heat and power (CHP) unit power output, EVs' charging power, EH's battery injection power, and G2SSH energy exchange. Additionally, there are demands for electrical energy balancing, including the desalination unit, EVs' consumption power, SSH2G energy exchange, subway's load, and EH's battery consumption power, as stated in (20). For heat balancing within the SSH (21), the sources of heat energy are the CHP unit and boiler, while the demands consist of the absorption chiller and the required heat consumption for each SSH station. Similarly, the cooling energy balancing (22) involves the SSH's cooling load at each station as the demand and the absorption chiller as the source of cooling energy. Furthermore, it's important to address the water energy balancing (28) within the SSH. The water demands include the SSH's connection to the water grid and the water loads at SSH stations. The water energy sources are the water grid connected to the SSH and the combination of sea water and the desalination unit.

- **Electricity grid of EH**
- EH's injection powers

$$\underline{P}^{EH}_{s,t} \le P^{EH}_{s,t} \le \overline{P}^{EH}_{s,t}, \qquad \forall t \in \vartheta^t, \forall s \in \vartheta^s \tag{14}$$

$$\underline{S}^{ES}_s \le S^{ES}_{s,t} \le \overline{S}^{ES}_s, \qquad \forall t \in \vartheta^t, \forall s \in \vartheta^s \tag{15}$$

$$S^{ES}_{s,t} = \left(1 - \alpha^{loss}_e\right) S^{ES}_{s,t-1} + P^{ch}_{s,t} - P^{dch}_{s,t}, \qquad \forall t \in \vartheta^t, \forall s \in \vartheta^s \tag{16}$$

$$\frac{1}{\eta^{ch}_e}\underline{P}^{ES} I^{ch}_{s,t} \le P^{ch}_{s,t} \le \frac{1}{\eta^{ch}_e}\overline{P}^{ES} I^{ch}_{s,t}, \quad \forall t \in \vartheta^t, \forall s \in \vartheta^s \tag{17}$$

$$\eta^{dch}_e \underline{P}^{ES} I^{dch}_{s,t} \le P^{dch}_{s,t} \le \eta^{dch}_e \overline{P}^{ES} I^{dch}_{s,t}, \quad \forall t \in \vartheta^t, \forall s \in \vartheta^s \tag{18}$$

$$0 \le I^{ch}_{s,t} + I^{dch}_{s,t} \le 1, \qquad \forall t \in \vartheta^t, \forall s \in \vartheta^s \tag{19}$$

- Electrical energy balancing

$$P^{E_{eh}}_{s,t} + P^{Des}_{s,t} + P^{E2SSH\_c}_{s,u,f,t} + P^{ch}_{s,t} = \eta^T_e P^{EH}_{s,t} + \eta^{GtoE}_{chp} P^{Gas_{chp}}_{s,t} + P^{dch}_{s,t} + P^{E2SSH\_d}_{s,u,f,t} + P^{rg}_{s,t}, \ \forall t \in \vartheta^t, \forall s \in \vartheta^s \tag{20}$$

- **Heat grid of EH**
- Heat balancing

$$P^{H_{Total}}_{s,t} = \eta^{GtoH}_{chp} P^{Gas_{chp}}_{s,t} + \eta^{GtoH}_{boi} P^{Gas_{boi}}_{s,t}, \quad \forall t \in \vartheta^t, \forall s \in \vartheta^s \tag{21}$$

$$P^{C_{eh}}_{s,t} = \eta_c \times \left(P^{H_{Total}}_{s,t} - P^{H_{eh}}_{s,t}\right), \qquad \forall t \in \vartheta^t, \forall s \in \vartheta^s \tag{22}$$

$$P^{GasIN}_{s,t} = P^{Gas_{chp}}_{s,t} + P^{Gas_{boi}}_{s,t}, \qquad \forall t \in \vartheta^t, \forall s \in \vartheta^s \tag{23}$$

- CHP and boiler units' Limitations

$$\eta^T_e P^{EH}_{s,t} \le C_s{}^T, \qquad \forall t \in \vartheta^t, \forall s \in \vartheta^s \tag{24}$$

$$\eta^{GtoH}_{chp} P^{Gas_{chp}}_{s,t} \le C_s{}^{CHP}, \qquad \forall t \in \vartheta^t, \forall s \in \vartheta^s \tag{25}$$

$$\eta^{GtoH}_{boi} P^{Gas_{boi}}_{s,t} \le C_s{}^{Boi}, \qquad \forall t \in \vartheta^t, \forall s \in \vartheta^s \tag{26}$$

$$\eta_c \times \left(P^{H_{Total}}_{s,t} - P^{H_{eh}}_{s,t}\right) \le C_s{}^{Ch}, \qquad \forall t \in \vartheta^t, \forall s \in \vartheta^s \tag{27}$$

The energy exchange constraint of the SSH interaction with the grid is expressed in (14). Constraints regarding the SSH unit's battery are represented in (15)-(19). Eq. (23) indicates the required consumption gas power for the SSH unit. The transformer capacity limit within the SSH unit is shown in (24). Capacity limits for the CHP and boiler are considered in (25) and (26) respectively. Furthermore, the constraint (27) specifies the capacity limit of the absorption chiller (Roustai et al., 2018). Constraints related to the water balancing of the network can be summarized as follows:

- **Water grid of EH**
- water energy balancing

$$Vol^{ST}_{s,t} = Vol^{ST}_{s,t-1} + W^{OD}_{s,t} + W^{Grid}_{s,t} - W^{Subway}_{s,t} \ \forall t \in \vartheta^T, \forall s \in \vartheta^s \tag{28}$$

$$\underline{Vol}^{ST}_s \le Vol^{ST}_{s,t} \le \overline{Vol}^{ST}_s \qquad \forall t \in \vartheta^T, \forall s \in \vartheta^s \tag{29}$$

$$Vol^{DT}_{s,t} = Vol^{DT}_{s,t-1} + W^{ID}_{s,t} - W^{OD}_{s,t} \qquad \forall t \in \vartheta^T, \forall s \in \vartheta^s \tag{30}$$

- water tanks' Limitations

$$0 \le Vol^{DT}_{s,t} \le \overline{Vol}^{DT}_s \qquad \forall t \in \vartheta^T, \forall s \in \vartheta^s \tag{31}$$

$$\underline{W}^{ID}_s . I^D_{s,t} \le W^{ID}_{s,t} \le \overline{W}^{ID}_s . I^D_{s,t} \qquad \forall t \in \vartheta^T, \forall s \in \vartheta^s \tag{32}$$

$$0 \le W^{OD}_{s,t} \le \overline{W}^{ID}_s \qquad \forall t \in \vartheta^T, \forall s \in \vartheta^s \tag{33}$$

$$P^{Des}_{s,t} = W^{ID}_{s,t} . CF^{Des} \qquad \forall t \in \vartheta^T, \forall s \in \vartheta^s \tag{34}$$

The capacity limits of the first and secondary water tanks in the SSH unit are presented in (29)-(31). The input and output capacities of the desalination unit are represented by (32)-(33), and the power required for the desalination unit is expressed in (34).

The operating costs for the grid, water, and gas are shown in (35)-(37), while the investment cost and profit gains from the energy selling of the SSH unit are indicated in (37)-(38).

$$cost_{Grid} = \sum_{s,t} \left(P^{EH}_{s,t}\right) \times price_{Grid} \tag{35}$$

$$cost_{Water} = \sum_{s,t} \left(W^{Subway}_{s,t}\right) \times price_{Water} \tag{36}$$

$$cost_{Gas} = \sum_{s,t} \left(P^{GasIN}_{s,t}\right) \times price_{Gas} \tag{37}$$

$$cost_{Inv} = \sum_s \begin{pmatrix} C_s{}^{CHP} . price_{InvCHP} + C_s{}^{Boi} . price_{InvBoi} + \\ C_s{}^T . price_{InvT} + \overline{S}^{ES}_s . price_{InvES} + C^{Ch}_s . price_{InvCh} \end{pmatrix} \tag{38}$$

$$Prof_{SSH2E} = \sum_{s \in \vartheta^s, u \in \vartheta^u, t \in \vartheta^t \ f \in \vartheta^f} Bp2_{s,t} \times \left(P^{E2SSH\_c}_{s,u,f,t} - P^{E2SSH\_d}_{s,u,f,t}\right) \tag{39}$$

2.3. Objective function of smart grid

As modeled in (40), the energy exchanges mentioned earlier impact the overall cost of the smart city. This cost comprises the investment cost, as well as the costs associated with the electrical grid, water, and gas. It also includes the profits from the energy exchange between SSH and EVs, as well as the EVs themselves. Constraint (41) establishes the power balance among the various segments of the smart grid within the smart city.

$$\text{Objective Function} : cost_{Total} = cost_{Grid} + cost_{Water} + cost_{Gas} + cost_{Inv} - Prof_{SSH2E} - Prof_E \tag{40}$$

Constraint

$$P^{Grid}_{Transaction} = Load^{Grid} - P^{Microgrid} - \sum_{s \in \vartheta^s, f \in \vartheta^{fl}, t \in \vartheta^t} P^{E2G}_{f,t} + P^{EH}_{s,t} \tag{41}$$

3. Security framework

Recently, the progress made in high-tech communication systems has significantly propelled the prominence of the smart city concept in power systems. Consequently, ensuring the security of data and energy exchanges within the system's nodes or agents has become a new challenge. In response, the use of blockchain technology has garnered considerable attention due to its decentralized and cryptographically secure structure (Liang et al., 2018). Unlike the centralized nature of the prevailing data transmission platform, known as Supervisory Control and Data Acquisition (SCADA), where all system data is broadcasted to a central node, blockchain technology enables data transactions through decentralized ledgers. All nodes in the system are involved in the process independently. Each node or agent in the system is assigned a private and a public key. By employing blockchain technology, nodes produce blocks that are authenticated and secured by a hash address (HA). These blocks are subsequently transmitted to other nodes in the network. The node's data block is encrypted using its private key and can be decrypted by other nodes using the public key, reducing the risk of data attacks. However, the challenges of HA generation in systems with numerous nodes and the cyclic nature of data transactions pose obstacles for the blockchain method. Recently, to enhance efficiency, security, and privacy, directed acyclic graph (DAG) approach has been introduced (Wang et al., 2019) to separate the cyclic blockchain into distinct components or categories: public, private, and transaction blockchains. DAG approach eliminates the cyclic form of the common blockchain and reduces the risk of unauthorized access to system data transactions.

Accordingly, this paper implements the DAG concept within a smart city composed of different sections, each requiring energy exchanges for its own benefit. The data transactions between these sections are facilitated through the DAG procedure as depicted in Fig. 2. It is important to note that in this paper, HA generation utilizes a 32-byte SHA-256 hash function constructed with the letters A-F and numbers 0–9 following the guidelines stated in (Liang et al., 2018). In each section of the smart city, various systems are present, each equipped with a sensor that transmits data to the Data and Energy Management Center (DAEMC) of that section. The DAEMC collects and transmits all sensor-related data for a section through a data block. This procedure is replicated in other sections and agents of the system.

The public, private, and transaction data of each section are directed and transacted within their respective public, private, and transaction blockchains. This approach enables secure energy exchanges among all nodes or agents and significantly reduces the risk of data manipulation. The goal is to facilitate the sharing of information regarding all energy exchanges among different active members.

4. Intelligent priority selection algorithm

This paper presents a novel algorithm for optimizing the assignment of charging stations in the smart city's metro system, considering its nonlinearities. Traditional optimization techniques based on mathematical programming or heuristic optimization methods often suffer from lengthy solving times and insufficient precision. To address these limitations, this paper proposes a robust approach that leverages stochastic search to enhance precision and simultaneously reduce overall runtime. From a statistical perspective, the definition for the count of combinations when selecting n items out of N is as follows:

$$\binom{N}{n} = \frac{N!}{(n!).(N-n)!} \tag{42}$$

While a brute force search would yield precise results, it is time-consuming due to the extensive range of samples. To address this issue, the proposed model, as shown in Fig. 3, suggests intelligently limiting the sample space as outlined in the following:

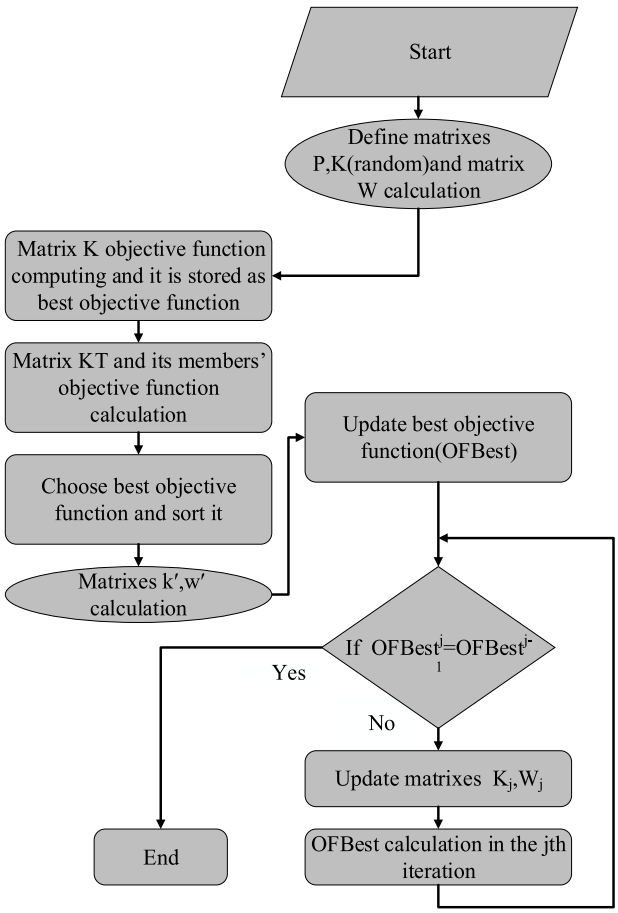

Fig. 3. The flowchart of the IPS algorithm.

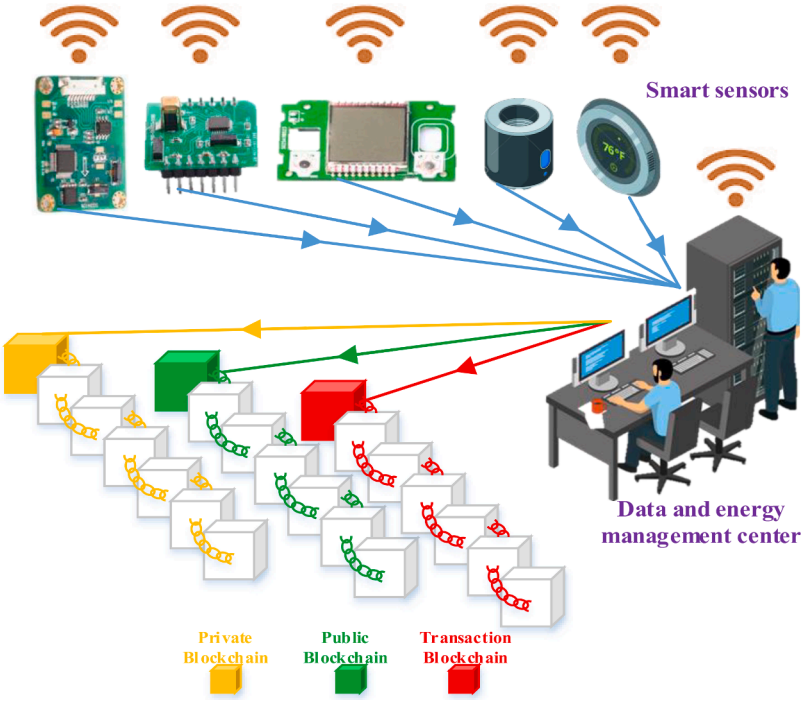

Fig. 2. The data transaction framework based on DAG.

Step 1: First, let the optimal values for the problem be assumed to reside in the primary set *P*. In the initial step, the vector *K* matrix for the control variables is randomly defined. The set *W* represents the remaining candidate points (*P* - *K*). Next, sets comprising *K* members for each member in W are generated, thereby replacing all possible sets. This process results in the formation of *KT* matrix. Moving forward, components of *H* are computed through substituting the corresponding element *i* of *W* in *K*, then the optimum solution is chosen from the members of H_{W_i}, denoted as $F^{best}_{W_1,K_n^{'}}$, as defined in (46). It is worth noting that $K_n^{'}$ in (46) represents the n-th element of *K*, which is substituted by the elements of *W*.

$$P = [p_1, ..., p_N] \tag{43}$$

$$K = [k_1, ..., k_n] \tag{44}$$

$$W = [w_1, ..., w_m] \tag{45}$$

$$KT = \begin{bmatrix} \overbrace{\begin{matrix} \overset{\neg k_1 = k_1^{'}}{\uparrow} & & & \\ w_1 & k_2 & ..... & k_n \\ & \overset{\neg k_2 = k_2^{'}}{\uparrow} & & \\ k_1 & w_1 & ..... & k_n \\ & & & \overset{\neg k_n = k_n^{'}}{\uparrow} \\ k_1 & k_2 & ..... & w_1 \\ & & \underset{F(H_{w_1}) = F^{best}_{w_{1,k_1^{''}}}}{\downarrow} & \end{matrix}}^{H_{w_1}} \cdots \overbrace{\begin{matrix} \overset{\neg k_1 = k_1^{'}}{\uparrow} & & & \\ w_m & k_2 & ..... & k_n \\ & & & \\ & & & \\ & & & \\ & & & \overset{\neg k_n = k_n^{'}}{\uparrow} \\ k_1 & k_2 & ..... & w_m \\ & & \underset{F(H_{wm}) = F^{best}_{w_{m,k_m^{''}}}}{\downarrow} & \end{matrix}}^{H_{w_m}} \end{bmatrix}$$

$$H_{w_i} = [H_{w_1}, H_{w_2}, ..., H_{w_m}] \qquad \forall i \in \Omega^i$$

$$k_M^{''} = [k_1^{'}, k_2^{'}, ..., k_n^{'}] \qquad \forall M \in \Omega^M \tag{46}$$

The elements of H_{W_i}, as depicted in (47)-(48), are organized based on the value of the objective function. Based on the values of the objective functions, the components of *W* are ranked.

The $W_j^{'}$ is shown as an array of the components of *W* (49) discussed earlier in this thread. The $W_j^{'}$ is shown as an array of the components of *W* (49) discussed earlier in this thread. This approach is also applicable to the set $K_j^{''}$ (50). Subsequently, the optimal solution for $W_1^{'}$ is picked as (51).

$$F_m^{best} = \left[F^{best}_{w_{1,k_1^{''}}} \quad ... \quad F^{best}_{w_{m,k_m^{''}}} \right]^T \qquad \forall m \in \Omega^m \tag{47}$$

$$F^{best\_sort} = \left[F^{best}_{w_1^{'} \to k_1^{''}} \quad ... \quad F^{best}_{w_m^{'} \to k_m^{''}} \right]^T \tag{48}$$

$$w_j^{'} = [w_1^{'}, ..., w_m^{'}] \qquad \forall m \in \Omega^m \tag{49}$$

$$k_j^{''} = [k_1^{''}, ..., k_m^{''}] \qquad \forall m \in \Omega^m \tag{50}$$

$$F = F^{best}_{w_1^{'} \to k_1^{''}} \tag{51}$$

Step 2: At this stage, the new KT (KT_r^{new}) is obtained. The updating process of W_j is initiated based on (52), utilizing the components of W_j. In the earlier iteration, $W_1^{'}$ was the best solution, and in this step, $W_2^{'}$ is initialized as described in (52). The generation of $[\![K1_j^{new}$ involves removing the $k_j^{''}$ and $w_j^{'}$ components from K_j (53). Like (46), the new component of KT_r^{new} is derived from all these possible sets, resulting from replacing the components of W_j with the component of $K1_j^{new}$. In KT_r^{new} and $w_j^{'}$, the combination of sets is represented as ψ_r, where *r* ranges from 1 to *m* - *j*. Here, *j* signifies the number of iterations, and *m* is a constant value that represents the matrix length of *W* in the initial step, as stated in (54). For each member of ψ_r, the objective value is calculated, and the optimal outcome of the objective function ($F1^{Best}$) and its associated component are stored as (55) and (56), respectively, in the matrix ψ_r (ψ^{Best}). In each iteration, K is modified by ψ^{Best} according to (57).

$$W_j = w_{j+1}^{'} \qquad \forall j \in \Omega^j \tag{52}$$

$$K1_j^{new} = \left\{ x | x \in K_j, x \neq k_j^{''}, x \neq w_j^{'} \right\} \qquad \forall j \in \Omega^j \tag{53}$$

$$\psi_r = KT_r^{new} \cup w_j^{'} \qquad r = \{1, 2, ..., m - j\} \tag{54}$$

$$F1_r = f(\psi_r) \tag{55}$$

$$F_j = F1^{Best} \qquad \forall j \in \Omega^j \tag{56}$$

$$K_j = \psi^{Best} \qquad \forall j \in \Omega^j \tag{57}$$

Step3: Among the other components, the optimal one is selected as the final component in each iteration.

$$F^{best\_total} = F^{Best} \tag{58}$$

5. Simulation results

Here, the performance of the proposed model is evaluated. The studied smart city is comprised of various sections, including EVs, smart grid, microgrid, and SSH (Alrumayh & Almutairi, 2023; Mohamed et al., 2023). The specifications of the EVs are presented in Table 6. Traffic jams (Seyedyazdi et al., 2019; Sánchez-Martín et al., 2015) and charging lines along different paths are considered in the urban transportation network. The microgrid (Javidsharifi et al., 2018) includes a wind park, PV power plant, tidal unit, and fuel cell. The specifications of the smart grid are taken from Calvillo et al. (2017). The SSH consists of the subway, EH (including CHP, boiler, storages, desalination (Ghaffarpour et al., 2018), and absorption chiller). Information regarding the gas and water grids is sourced from Ghaffarpour et al. (2018). The prices for water, gas, heat, cooling, and electricity within the SSH are determined as described in (Roustai et al., 2018). The important characteristics of source units and demands into SSH are illustrated by Table 1–5, and Figs. 4–6. The SSH allocation problem involves optimizing the selection of three locations for SSH construction out of six candidate sites. This selection process depends on two critical factors. Firstly, the subway's specifications, including the BE, number of EVs, and their access times to the subway stations. Secondly, the EH's specifications encompass the heat, water, cooling, and power consumption of the subway stations. Notably, the EH supplies the electrical demand of the desalination unit and the subway's load. Here, five case studies are analyzed for the smart city as follows.

Case I: *Analysis of EVs' energy exchange*

EVs can engage in energy exchanges with the smart grid and SSH. This paper conducts on optimizing SSH allocation to maximize profit, considering factors like EVs (number, access time, transaction price,

Table 1
The charactristic of CHP units.

Capacity(kW)	η_{ge}^{CHP} (%)	η_{gh}^{CHP} (%)
100	43	53

Table 2
The charactristic of ES units.

Capacity(kW)	α_e^{loss}(%)	η_e^{dch}(%)	η_e^{ch}(%)
50	2	95	95

Table 3
The charactristic of desalination units.

CF^{Des}	Capacity(m^3)		IC($/$m^3$)	
(KW /Liter)	FWT	DT	FWT	DT
3.5	100	50	200	166

Table 4
The charactristic of boiler units.

Capacity(kW)	η_{gh}^{B}(%)
100	78

Table 5
The charactristic of transformers.

Capacity(kW)	η_e^{Tr} (%)
80	98

Table 6
Specifications of the EVs fleets ssin smart city (Mohamed et al., 2023).

Fleet No.	No. EVs	Access Time	Capacity (kWh)		(dis)charge rate (kW)	
			Min	max	min	max
1	40	7–8,12–13,15–17	219	1644	7.3	292
2	63	7–10,12–14,17–19	263	1973	7.3	496
3	54	7–10,12–14,17–19	251	1902	7.3	386
4	33	12–14,16–18	208	1610	7.3	234
5	54	7–10,12–14,17–19	251	1902	7.3	386
6	39	7–9,12–14,16–18	219	1644	7.3	292

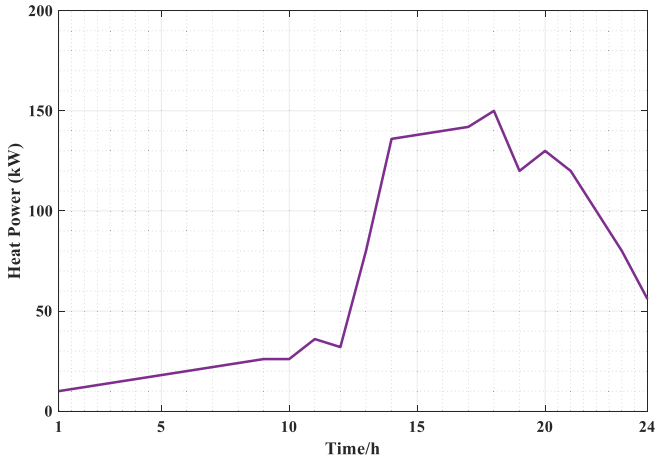

Fig. 4. Heat demand of SSH.

traffic density) and SSH stations (breaking energy, water/heat/cooling demands, EH costs, water/gas prices). The optimal allocation selects SSH (2), SSH (3), and SSH (5) among six candidates. Figs. 7 and 8 depict energy exchanges of EV fleets with the smart grid and allocated SSH. All six EV fleets connect to the smart grid, while only the allocated SSH

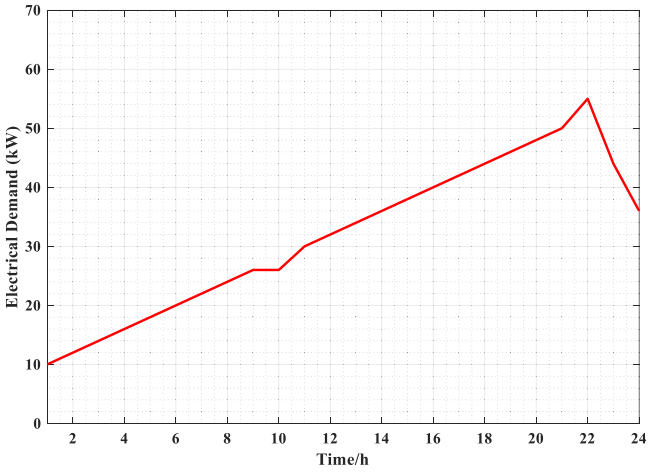

Fig. 5. Electrical demand of SSH.

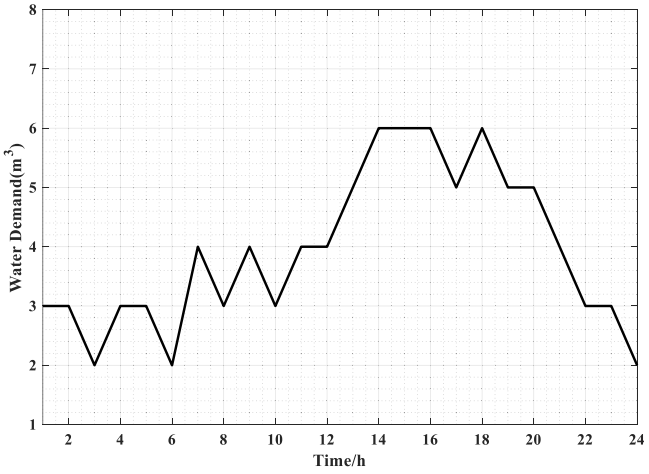

Fig. 6. Water demand of SSH.

serves EVs. Positive values imply EV power consumption, negative values imply power injection. EVs prioritize charging from the grid and injecting stored energy into SSH during specific hours for financial efficiency.

Case II: *Energy exchange of the smart grid and microgrid*

As an integral component of a smart city, the microgrid plays a crucial role in reducing overall operational costs through energy exchanges with the smart grid. Fig. 9 illustrates the energy exchanges between the smart grid and microgrid. Positive values represent energy generation, while negative values indicate energy consumption. The performance of the smart grid experiences a decline at $t = 6$ and reaches zero power generation at $t = 7$, coinciding with the start of power generation by the PV unit. Furthermore, during $t = 10$ to 14, the smart grid strategically prioritizes power consumption from the microgrid, which offers the lowest cost of operation.

Case III: *Performance analysis of the SSH in different study cases*

The production sources in the SSH involve battery EVs' charging power, CHP power, EH's battery discharging power, G2SSH energy exchange, and desalination unit. The electrical balancing of the SSH is related to the demands of the desalination unit, EVs' charging power, SSH2G energy exchange, subway's load, and EH's battery charging power. Regarding the heat balancing of the SSH, it encompasses the CHP

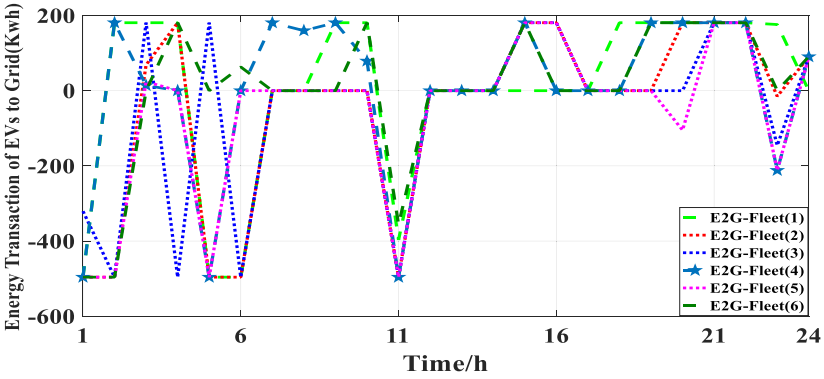

Fig. 7. Energy exchange of the EVs to grid.

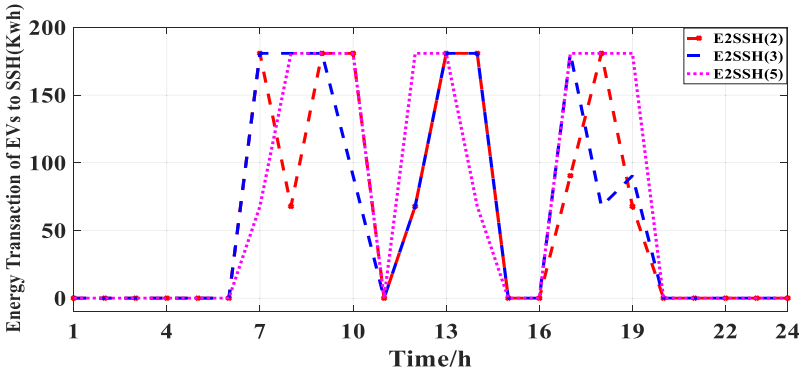

Fig. 8. Energy exchange of the EVs to SSH.

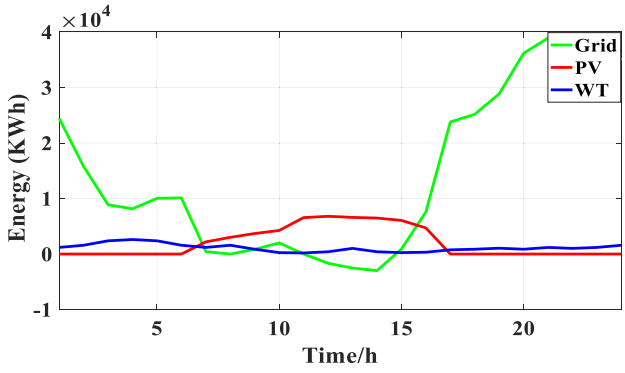

Fig. 9. The energy exchanges of the smart grid.

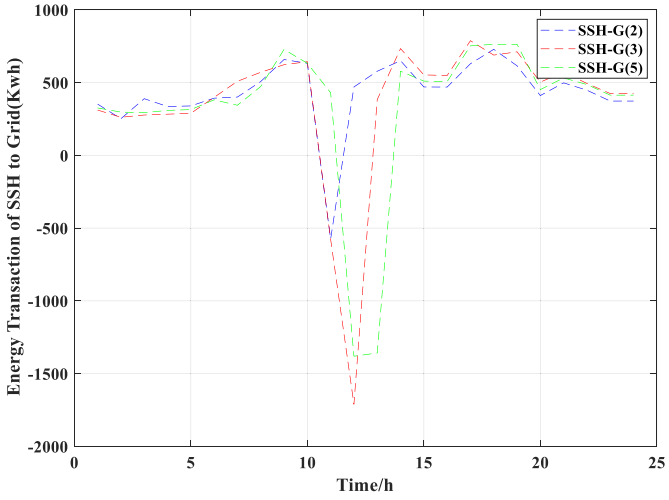

Fig. 10. Energy exchange of the SSH to grid.

unit and boiler as sources of heat energy, while the absorption chiller and the heat consumption requirements for each station within the SSH represent the demands for heat energy. Another aspect that requires attention is the balancing of cooling energy. Similarly, the cooling energy demands consist of the cooling load of each station within the SSH, while the absorption chiller serves as the source of cooling energy. Furthermore, the water demands include the water grid supplying the SSH and the water loads of SSH's stations. The water energy sources involve the combination of sea water and the desalination unit, as well as the water grid supplying the SSH.

Fig. 10 illustrates the energy exchange of electrical energy between the SSH and the grid. Positive values indicate energy generation by the SSH, while negative values represent energy consumption by the SSH. The figure clearly demonstrates an increase in electrical energy consumption, including the subway's electrical load and the desalination unit's power, during hours 11–14. This energy consumption is consistent with the data shown in Fig. 8, where the proposed energy consumption is utilized for desalinating sea water and selling it to the water grid.

It is also noteworthy that within SSH (2), the water energy has not been transferred to the grid due to its higher water demand compared to SSH (4) and (5). Figs. 12 and 13 depict the electrical power generation of the CHP and the power consumption of the desalination unit, respectively. Fig. 14 demonstrates an increase in power generation during $t =$ 12 - 15. During these hours, the gas price is lower compared to the water price, making it preferable to consume more gas power to generate more electrical power. This, in turn, leads to increased water production by

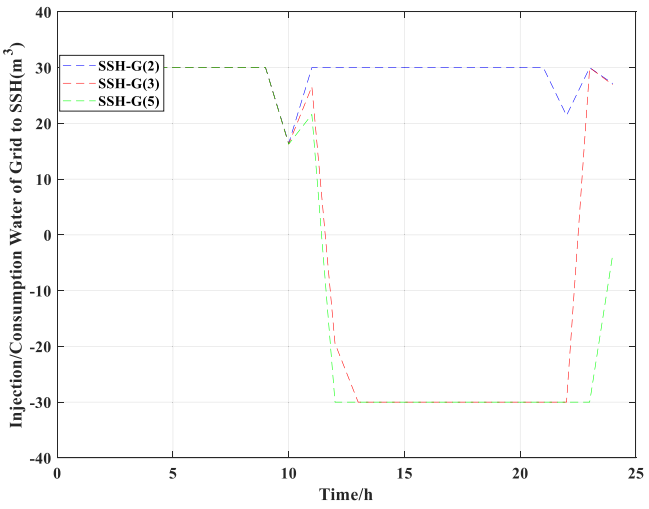

Fig. 11. Water energy exchange of the SSH to grid.

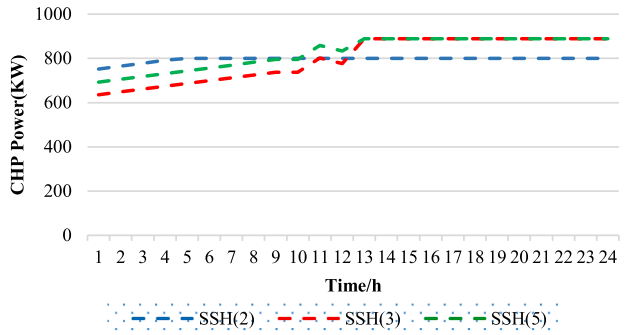

Fig. 12. CHP power generation.

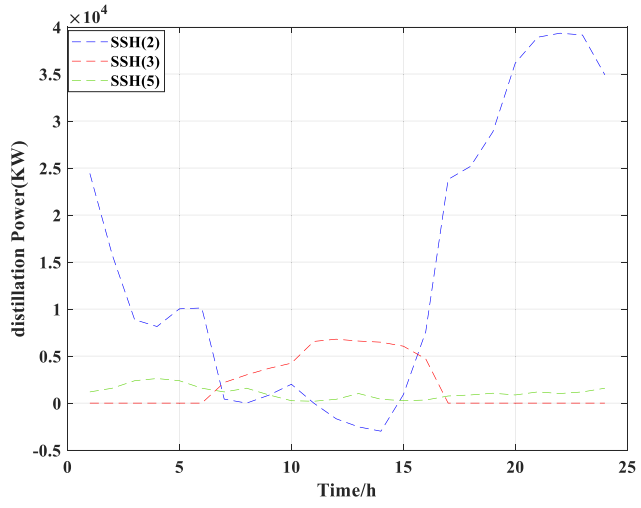

Fig. 13. Desalination unit power consumption.

the desalination unit. To maximize profits, the surplus desalinated water can be sold to the water grid. Fig. 11 explicitly illustrates this definition.

Table 7 compares different scenarios of the SSH. Scenario 1 assumes that the subway operates without EH, while Scenario 2 represents non-synergistic operation of the EH, where the EH and the subway operate independently. Scenario 3 considers the operation of the SSH, as proposed in this paper. The results in Scenario 3 are remarkably similar to those in Scenario 1, where water, heat, and cooling demands are directly supplied by the water and gas grids. They also show similarities to Scenario 2, where the independently operated EH is responsible for supplying these demands. However, the costs and profits in Scenario 3 have decreased and increased, respectively, compared to the results in Scenarios 1 and 2.

Case IV: *Analysis of the IPS algorithm*

In Case IV, the analysis of the IPS algorithm is conducted, which serves as a novel method utilized to determine the optimal location of the SSH unit. This part focuses on validating the IPS algorithm. The convergence of the IPS algorithm is demonstrated in Fig. 14. It is observed that, after 10 iterations, the proposed optimization method successfully identifies stations 2, 3, and 5 as the optimal locations for the SSH. To assess the performance of the proposed method, a comparison is made with various optimization approaches (Alrumayh & Almutairi, 2023) in Table 8. Several items are compared, including the best, average, and worst solutions, as well as the CPU process time. The IPS method demonstrates a significantly lower iterative process time for finding the solution, as compared to other optimization methods (Kavousi-Fard & Khosravi, 2016). For instance, the CPU execution time has been reduced by 66.77 %, 54.15 %, and 50.12 % in comparison with the NPSO-LRS, HDE, and IGAMU methods (Alrumayh & Almutairi, 2023), respectively. Moreover, the IPS algorithm exhibits an approximate tendency for the answer deviation to approach zero.

6. Discussions

In this research, by utilizing the concept of SSH, the operating costs of water, electricity, and heat networks were significantly reduced, and the profits derived from simultaneously considering various energies in the infrastructure of the SSH increased drastically compared to the old methods. On the other hand, by employing the IPS method, the system convergence time decreased, and the accuracy of the issue also

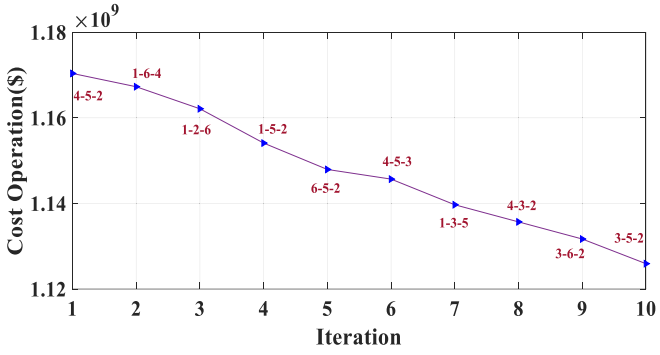

Fig. 14. Convergence diagram of the IPS algorithm.

Table 7
Different scenarios of the SSH operation.

Total Cost of →	Water grid	Gas consumption	Profit of energy exchange with grid	Investment	Energy exchange with EVs
Without Hub (scenario 1)	72.391370×10^6	16,899.600	19.644647×10^6	–	2.445×10^5
Non synergism Hub (scenario 2)	43.448400×10^6	17,820.473	42.315925×10^6	81,205,000	1.250×10^5
SSH (scenario 3)	13.874759×10^6	14,850.390	87.668385×10^6	81,205,000	1.123×10^5

Table 8
Performance evaluation of the IPS algorithm.

Method	Best	Average	Worst	CPU (min)
IFEP	1.138246×10^9	1.138654×10^9	1.139125×10^9	35.43
ESO	1.13458×10^9	1.134894×10^9	1.139125×10^9	23.87
PSO-LRS	1.13458×10^9	1.137654×10^9	1.138256×10^9	25.15
Improved GA	1.13458×10^9	1.137654×10^9	1.138256×10^9	NA
HPSOWM	1.129871×10^9	1.1312547×10^9	1.133985125×10^9	30.54
IGAMU	1.128246×10^9	1.1312547×10^9	1.133985125×10^9	30.85
HDE	1.128246×10^9	1.13012514×10^9	1.1312547×10^9	22.356
NPSO-LRS	1.12598654×10^9	1.13012514×10^9	1.1312547×10^9	20.548
IPS	$\mathbf{1.125916773 \times 10^9}$	$\mathbf{1.125916773 \times 10^9}$	$\mathbf{1.125916773 \times 10^9}$	**10.25**

increased. Another issue is maintaining the security of energy exchange between different components of the energy network, which was addressed using the blockchain method.

7. Conclusions

This paper presented a novel concept for the smart transportation system (STS) known as the subway synergism hub (SSH). By integrating the EH within subway stations, the SSH enables the simultaneous operation of various systems, including the smart grid, water grid, gas grid, microgrid, and EVs. This integrated approach effectively addresses the energy demands of a smart city, encompassing electrical, water, heat, and cooling energy requirements. Furthermore, the paper addressed the optimal allocation of the SSH unit to ensure efficient operational management. To achieve this, an innovative mathematical-based intelligent priority selection algorithm was developed to tackle the allocation problem. Also, the IPS method shows a significantly shorter iterative process time for finding solutions compared to other optimization methods. Furthermore, the CPU execution time has been decreased by 66.77 %, 54.15 %, and 50.12 % when compared to the NPSO-LRS, HDE, and IGAMU methods. The results indicate that by considering the proposed SSH in this article and with an equal investment cost, water grid costs have been reduced by 80.83 % and 68.07 % compared to scenarios where the EH is not present and where the EH is present, respectively. Additionally, the security of data and energy exchanges within the smart city was investigated using a directed acyclic graph approach and blockchain technology. These measures provide a highly secure platform for the smart city, safeguarding the integrity of its systems. Overall, this research presents a promising framework for enhancing the efficiency and security of smart transportation systems within smart cities.

CRediT authorship contribution statement

Mahmoud Roustaei: Writing – original draft, Software, Methodology, Investigation, Conceptualization. **Taher Niknam:** Conceptualization, Supervision, Validation, Writing – review & editing. **Jamshid Aghaei:** Conceptualization, Supervision, Writing – review & editing. **Morteza Sheikh:** Software, Methodology, Data curation. **Hossein Chabok:** Visualization, Software, Methodology. **Abdollah Kavousi-Fard:** Writing – review & editing, Conceptualization. **Vahid Vahidinasab:** Writing – review & editing, Formal analysis. **Josep M. Guerrero:** Writing – review & editing.

Declaration of competing interest

The authors declare that they have no known competing financial interests or personal relationships that could have appeared to influence the work reported in this paper.

Data availability

Data will be made available on request.

References

Adinolfi, A., Lamedica, R., Modesto, C., Prudenzi, A., & Vimercati, S. (1998). Experimental assessment of energy saving due to trains regenerative braking in an electrified subway line. *IEEE Transactions on Power Delivery, 13*, 1536–1542.

Aguado, J. A., Racero, A. J. S., & de la Torre, S. (2016). Optimal operation of electric railways with renewable energy and electric storage systems. *IEEE Transactions on Smart Grid, 9*, 993–1001.

Alrumayh, O., & Almutairi, A. (2023). Novel secured distributed energy management structure for solar based smart grids incorporating miners. *Solar Energy, 251*, 134–145.

Ashley, M. J., & Johnson, M. S. (2018). Establishing a secure, transparent, and autonomous blockchain of custody for renewable energy credits and carbon credits. *IEEE Engineering Management Review, 46*, 100–102.

Bridge, G., Bouzarovski, S., Bradshaw, M., & Eyre, N. (2013). Geographies of energy transition: Space, place and the low-carbon economy. *Energy Policy, 53*, 331–340.

Calvillo, C. F., Sánchez-Miralles, A., & Villar, J. (2016). Energy management and planning in smart cities. *Renewable and Sustainable Energy Reviews, 55*, 273–287.

Calvillo, C. F., Sánchez-Miralles, Á., & Villar, J. (2017). Synergies of electric urban transport systems and distributed energy resources in smart cities. *IEEE Transactions on Intelligent Transportation Systems, 19*, 2445–2453.

Geidl, M., Gaudenz, K., Favre-Perrod, P., Klockl, B., Andersson, G., & Frohlich, K. (2007). Energy hubs for the future. *IEEE Power and Energy Magazine, 5*(1), 24–30.

Ghaffarpour, R., Mozafari, B., Ranjbar, A. M., & Torabi, T. (2018). Resilience oriented water and energy hub scheduling considering maintenance constraint. *Energy, 158*, 1092–1104.

González-Gil, A., Palacin, R., Batty, P., & Powell, J. (2014). A systems approach to reduce urban rail energy consumption. *Energy Conversion and Management, 80*, 509–524.

Guo, Qun, Nojavan, Sayyad, Lei, Shi, & Liang, Xiaodan (2021). Economic-environmental analysis of renewable-based microgrid under a CVaR-based two-stage stochastic model with efficient integration of plug-in electric vehicle and demand response. *Sustainable Cities and Society, 75*, Article 103276.

Hui, Chu Xiao, Dan, Ge, Alamri, Sagr, & Toghraie, Davood (2023). Greening smart cities: An investigation of the integration of urban natural resources and smart city technologies for promoting environmental sustainability. *Sustainable Cities and Society, 99*, Article 104985.

Javidsharifi, M., Niknam, T., Aghaei, J., & Mokryani, G. (2018). Multi-objective short-term scheduling of a renewable-based microgrid in the presence of tidal resources and storage devices. *Applied Energy, 216*, 367-38.

Kavousi-Fard, A., & Khosravi, A. (2016). An intelligent θ-Modified Bat Algorithm to solve the non-convex economic dispatch problem considering practical constraints. *International Journal of Electrical Power & Energy Systems, 82*, 189–196.

Kavousi-Fard, A., Niknam, T., & Fotuhi-Firuzabad, M. (2015). Stochastic reconfiguration and optimal coordination of V2G plug-in electric vehicles considering correlated wind power generation. *IEEE Transactions on Sustainable Energy, 6*, 822–830.

Khayyam, S., Ponci, F., Goikoetxea, J., Recagno, V., Bagliano, V., & Monti, A. (2015). Railway energy management system: Centralized–decentralized automation architecture. *IEEE Transactions on Smart Grid, 7*, 1164–1175.

Khodayar, M. E., Wu, L., & Shahidehpour, M. (2012). Hourly coordination of electric vehicle operation and volatile wind power generation in SCUC. *IEEE Transactions on Smart Grid, 3*, 1271–1279.

Khosrojerdi, F., Taheri, S., Taheri, H., & Pouresmaeil, E. (2016). Integration of electric vehicles into a smart power grid: a technical review. In *Proc. Electrical Power and Energy Conference (EPEC), October*.

Liang, G., Weller, S. R., Luo, F., Zhao, J., & Dong, Z. Y. (2018). Distributed blockchain-based data protection framework for modern power systems against cyber attacks. *IEEE Transactions on Smart Grid, 10*, 3162–3173.

Liang, Xuedong, Zhan, Wenting, Li, Xiaoyan, & Deng, Fumin (2024). Unveiling causal dynamics and forecasting of urban carbon emissions in major emitting economies through multisource interaction. *Sustainable Cities and Society, 105326*.

Mehdizadeh, A., & Taghizadegan, N. (2017). Robust optimisation approach for bidding strategy of renewable generation-based microgrid under demand side management. *IET Renewable Power Generation, 11*(11), 1446–1455.

Mohamed, M. A., Almalaq, A., Awwad, E. M., El-Meligy, M. A., Sharaf, M., & Ali, Z. M. (2023). An effective energy management approach within a smart island considering water-energy hub. *IEEE Transactions on Industry Applications*. https://doi.org/10.1109/TIA.2020.3000704

Morvaj, B., Lugaric, L., & Krajcar, S. (2011). Demonstrating smart buildings and smart grid features in a smart energy city. In *Proceedings of the 2011 3rd international youth conference on energetics (IYCE)* (pp. 1–8).

Mwasilu, F., Justo, J. J., Kim, E.-K., Do, T. D., & Jung, J.-W. (2014). Electric vehicles and smart grid interaction: A review on vehicle to grid and renewable energy sources integration. *Renewable and Sustainable Energy Reviews, 34*, 501–516.

Pournazarian, B., Abedi, M., Gharehpetian, G. B., & Pouresmaeil, E. (2019). Smart participation of PHEVs in controlling voltage and frequency of island microgrids. *International Journal of Electrical Power and Energy Systems, 110*, 510–522. Sep.

Roustai, M., Rayati, M., Sheikhi, A., & Ranjbar, A. (2018). A scenario-based optimization of Smart Energy Hub operation in a stochastic environment using conditional-value-at-risk. *Sustainable Cities and Society, 39*, 309–316.

Sánchez-Martín, P., Lumbreras, S., & Alberdi-Alén, A. (2015). Stochastic programming applied to EV charging points for energy and reserve service markets. *IEEE Transactions on Power Systems, 31*, 198–205.

Sarda, P., Chowdhury, M. J. M., Colman, A., Kabir, M. A., & Han, J. (2018). Blockchain for fraud prevention: A work-history fraud prevention system. In *2018 17th IEEE International Conference On Trust, Security And Privacy In Computing And Communications/12th IEEE International Conference On Big Data Science And Engineering (TrustCom/BigDataSE)* (pp. 1858–1863).

Seyedyazdi, M., Mohammadi, M., & Farjah, E. (2019). A combined driver-station interactive algorithm for a maximum mutual interest in charging market. *IEEE Transactions on Intelligent Transportation Systems*.

Wang, B., Dabbaghjamanesh, M., Fard, A. K., & Mehraeen, S. (2019). Cybersecurity enhancement of power trading within the networked microgrids based on blockchain and directed acylic graph approach. *IEEE Transactions on Industry Applications*.

Xiaping, Z., Shahidehpour, M., Alabdulwahab, A., & Abusorrah, A. (2015). Optimal expansion planning of energy hub with multiple energy infrastructures. *IEEE Transactions on Smart Grid, 6*(5), 2302–2311.

Xu, Yi-Peng, Liu, Run-Hao, Tang, Lu-Yuan, Wu, Hao, & She, Chen (2022). Risk-averse multi-objective optimization of multi-energy microgrids integrated with power-to-hydrogen technology, electric vehicles and data center under a hybrid robust-stochastic technique. *Sustainable Cities and Society, 79*, Article 103699.

Yang, X., Ning, B., Li, X., & Tang, T. (2014). A two-objective timetable optimization model in subway systems. *IEEE Transactions on Intelligent Transportation Systems, 15*, 1913–1921.